Ultra-compact 2-bit analog-to-digital convertor based on silicon photonic crystal waveguide

MASOUD MOHAMMADI[1], RAHIM KARAMI[2], MAHMOUD SEIFOORI[1], SAEED OLYAEE[1,2,*]
[1]*Faculty of Electrical Engineering, Shahid Rajaee Teacher Training University, Tehran, Iran*
[2]*Nano-photonics and Optoelectronics Research Laboratory (NORLab), Shahid Rajaee Teacher Training University, 16788-15811, Tehran, Iran*

This study aims to design and simulate a two-dimensional all-optical nonlinear analog-to-digital converter (ADC) using a set of power splitters, U-shaped, add/drop, and bus waveguides. In this work, the transmission and wavelength of output ports are managed by the length of the waveguide, number of coupling rods, nonlinear effects, and also the radius and refractive index of coupling and scattering rods. In this design, according to the nonlinear effects and the controlling parameters we can approximate the logic 0 and 1 states using the power transmission at the output ports. The finite-difference time-domain (FDTD) method is employed to investigate the transmission characteristics of the device for a variety of refractive indices. The output efficiency of the 2-bit converter is estimated as 80% and the footprint of the proposed structure is obtained to be 741 μm^2. The minimum quantized pulse width of the proposed structure is 0.7 ps. Considering this time delay, the conversion rate is estimated as much as 1430 Gb/s.

(Received June 14, 2023; accepted February 9, 2024)

Keywords: Analog-to-digital converter (ADC), Silicon photonic crystal, Interference, Nonlinear effect

1. Introduction

Nowadays, light-based technologies play a key role in the rapid development of information and communication speed. Devices that use photons, instead of electrons, as information carriers have higher bit rates, transmission efficiencies and bandwidth, protection against electromagnetic noise, reduced inter-channel interference, and higher rate than electronic systems [1-7]. Therefore, using optical technologies, instead of electronics, leads to a great revolution in the information exchange and telecommunication industry in the future [8-13]. In optical structures, all the communication steps should be done without the intervention of electronic structures in order to enjoy all the advantages of optical communication. Nowadays, ADCs are among the key elements of optical systems. These converters receive analog information and convert them into digital signals. Speed is among the most important limiting parameters of ADCs [1]. Given that according to the Nyquist criterion, the sampling frequency of the optical converter should be at least twice the frequency of analog signals, the speed problem of these optical ADCs has to be solved. The photonic crystal is among the most suitable structures that can be used to achieve an all-optical ADC [14, 15].

Optical ADCs are generally divided into two types. First, convertors based on the Nyquist criterion, and second the convertors which are working based on oversampling state. Oversampling converters are divided into two categories: Sigma-Delta analog-to-digital converter (SD-ADC) and ADC error correction. ADCs also use an internal encoding method. These methods support specific quantization and can encode output quickly. The three most important internal codes used nowadays include Thermometer, Gray, and Circular codes.

Nowadays, the use of new techniques to manage the logical “zero”/“one” states in the output ports of the optical converters based on nonlinear effects and the creation of key optical structures such as rings and waveguides is very important and practical. Numerous articles have examined the nonlinear effects of photonic convertors [15-17].

To be able to create the correct logic states at the output of analog-to-digital converters using the Kerr effect [18, 19], it is necessary that the structure of the presented converters be designed based on the interferometers [20-22], optical switches [23, 24], ring resonators [25, 26], nano-cavities and central waveguides [27-33]. This paper presents a two-bit analog-to-digital converter using the nonlinear Kerr effect. This converter is designed using a combination of waveguides with nano-ring resonators.

Geng *et al*. propose an all-optical analog-to-digital converter based on photonic ring resonators using nonlinear effects, which aimed to design an optical ADC with no upper limit for the input optical intensity when generating code “11” at the output ports [34]. Shamsi and Moradi presented analog-to-digital converters using nonlinear ring resonators. In this structure, nonlinear multiplexers could convert the analog input signal into

discrete levels of input optical intensity. The delay time of the structure was obtained as 4 ps [35].

Gandhi *et al*. presented analog-to-digital converters based on photonic crystals and proposed 1- and 2-bit ADCs which were suitable for integration. In the 2-bit converter, the maximum insertion loss was -5.5596 dB and the dimensions of the structure were reported to be 358 μm^2. In the 1-bit converter, the maximum insertion loss was -10.4576 dB and the dimensions of the structure were reported to be 118 μm^2 [28]. Jafari *et al*. proposed ADCs based on the Kerr effect. Given that the operating wavelength of this structure was 1550 nm, it was very suitable to be used in telecommunication systems. This structure was 42 μm^2 in size and had a sampling rate of 1 TB/s [18]. Mehdizadeh *et al*. presented a 2-bit ADC based on photonic cavities [36]. This structure consisted of two parts: (a) a nonlinear 3-channel multiplexer, and (b) an optical encoder. In the optical multiplexer, the input analog signal was converted into quantized surfaces based on the intensity. Then, the quantized surfaces were converted into binary codes by the optical encoder. The maximum sampling rate of the mentioned structure was up to 52 GS/s and its dimensions were about 924 μm^2 [37, 38].

In the present study, the finite-difference time-domain (FDTD) method was used to simulate the structure and extract the output spectrum results. Also, the plane wave expansion (PWE) method was employed to investigate TE and TM modes and calculate the frequency eigenvalues and photonic band gap of the proposed structure [39, 40].

This paper is formed as follows. Section 2 focuses on the structure of the proposed ADC. In section 3 simulation results obtained are presented and discussed and finally the conclusions are drawn in section 4.

2. Proposed structure

In this study, a 2-bit all-optical ADC was analyzed, designed, and simulated. The proposed converter consists of a set of power splitters, U-shaped, add/drop, and bus waveguides which can be easily fabricated on a thin Si-on-Isolator (SOI) using the smart cut technique [41]. Fig.1 shows the structure of the proposed ADC and the key parameters in designing the proposed structure are listed in Table 1. The designed ADC was made of a square lattice of silicon dielectric rods with a refractive index of 3.46 at a wavelength of 1.55 μm. This structure consists of 29 dielectric rods in each X- and Z-direction in the air substrate. To have a proper response, the rod radius and lattice constant in this design were considered as 108 nm and 542 nm, respectively.

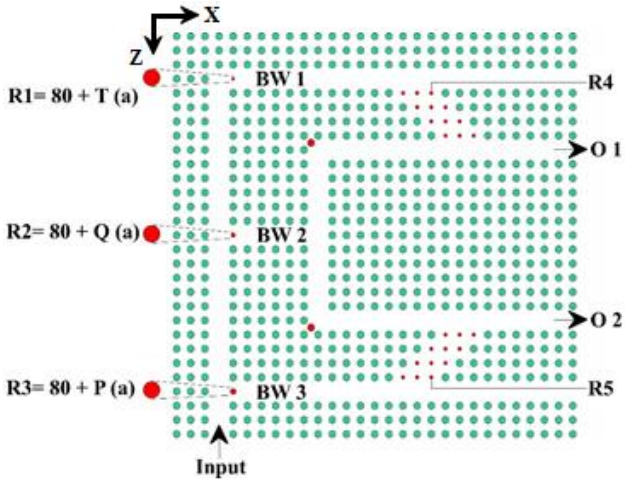

Fig. 1. The 2D schematic of the proposed analog-to-digital converter (color online)

The photonic band gap of the proposed structure is shown in Fig. 2. In this structure, the photonic band gap does not change with changes in the dimensions of the structure due to the scalability of the structure. The reason for the scalability of the structure is the dependence of the parameters on the lattice constant. According to Fig. 2, the ranges 705 nm ≤ λ≤ 731 nm and 1238 nm ≤ λ ≤ 1863 nm are considered as the band gap range for the proposed structure. The second bandgap range in TM mode is considered a suitable operating area for the design of optical devices in telecommunication networks due to its wide bandwidth.

Table 1. Design parameters of the proposed ADC

Parameter	Symbol	Quantity	Unit
Lattice constant	α	542	nm
Rods material	Si	-	-
Rods radius	r	108	nm
The refractive index of rods	n_{Si}	3.46	-
Background material	air	-	-
The refractive index of the background	n_{air}	1	-
Dimension	2DXZ	-	-
Lattice size	-	29×29	-
Rod shape	Circle	-	-
FDTD temporal grid (time step size)	cΔt	5	nm
The corresponding wavelength of the PBG	λ	1238-1863	nm
The normalized band gap (TM)	a\λ	0.279-0.420	
Center wavelength	λ0	1550	nm

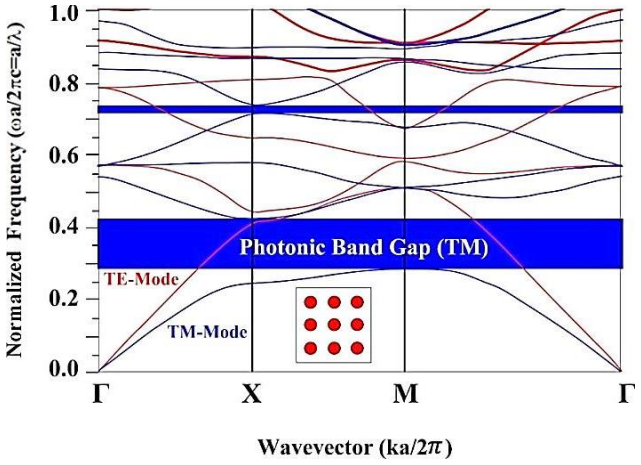

Fig. 2. The photonic band gap for the proposed 2D PhC structure (color online)

In the proposed structure, the changes in the refractive index and radius of R1, R2, R3, R4, and R5 are used to control the output. The proposed ADC is formed by two structures. The structure (1) is a power splitter. This splitter manages and controls the value of the transmission power towards the up and down bus waveguide and U-shaped waveguides using the diameters and refractive indices of 1, 2, and 3 dielectric rods. Because photonic crystal structures are highly sensitive to changes in refractive index, in this splitter, the main goal is to manage the output using changes in the radius of the dielectric rods. Fig. 3 illustrates the PC power splitter structure. Table 2 shows the key parameters in determining the value of power and output wavelength of the proposed splitter structure, including wavelength lengths, refractive index, and radius of the controlling dielectric rods.

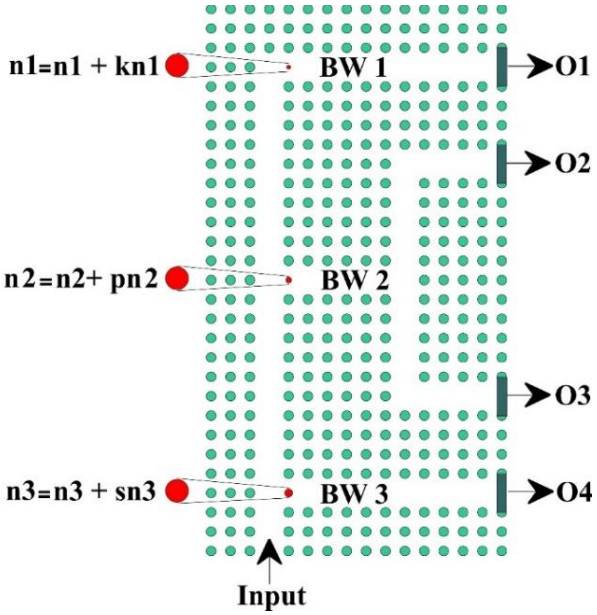

Fig. 3. PC power splitter based on bus and U-shaped waveguides (color online)

According to Table 2, the refractive index of the dielectric rods R1, R2, and R3 varies concerning changes in the input power intensity. These changes are expressed by three parameters K, p, and s in Table 2. These parameters create the nonlinear part of the Kerr effect in the dielectric rods. Due to these changes and the definition of the threshold level, the logic levels of "zero" and "one" are defined as the output of the structure. In this splitter, to control the output power of the ports, changes of parameters such as T, Q, P, K, p, and s have been used to make changes in the radius and refractive index of the input rods of the waveguides.

Table 2. The design parameters of the splitter

Parameter	Symbol	Quantity	Unit
The radius of rod (1)	R1	80 + T (a)	nm
The radius of rod (2)	R2	80 + Q (a)	nm
The radius of rod (3)	R3	80 + P (a)	nm
The refractive index of R1	n1	n1 + Kn1	-
The refractive index of R2	n2	n2 + pn2	-
The refractive index of R3	n3	n3 + sn3	-
Length of BW1	-	11a	nm
Length of BW2	-	5a	nm
Length of BW3	-	11a	nm

Fig. 4 shows the structure (2) which is a 4×2 demultiplexer. In this structure, the input power is divided into three power ranges using a power splitter structure. The power range related to the second waveguide is divided into two equal powers using U-shaped waveguide. In this demultiplexer structure, the output power of the ports is controlled using changes in the radius and refractive index of the dielectric coupling rods. The structure of this demultiplexer is designed entirely symmetrical for simplicity in the fabrication process and better control of the output. To reduce losses in the U-shaped waveguide, scattering rods are placed at 90 ° bends. Reducing losses using these rods will increase the output power.

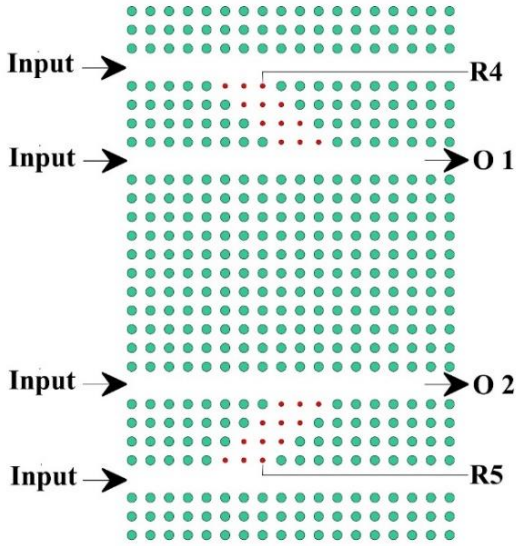

Fig. 4. PC demultiplexer based on nano-rods and waveguides (color online)

3. Simulation results

The interference effect on photonic crystals is used to optimize the output parameters of the proposed structure, which simplifies the structure design. The plane wave expansion method was employed to analyze the structure in terms of dispersion and photonic band gap range, and the FDTD method was employed to analyze the structure output spectrum. The FDTD method is a precise and powerful tool for modeling nano-scale optical devices. FDTD solves Maxwell's equations directly without any physical approximation, and the maximum problem size is limited only by the extent of the computing power available. If Eq. (1) is satisfied, FDTD time stepping formulas are stable numerically [42]:

$$\Delta t = \frac{1}{c\sqrt{(\Delta x)^2+(\Delta y)^2}} \quad (1)$$

where, c is the speed of light in vacuum, Δt is the time step, Δx, and Δy are mesh sizes in the x, and y directions, respectively.

One of the most vital parameters in the design of a photonic crystal device is the dimensions of the structure. Also, in these structures, due to the PBG, certain wavelengths can be propagated. Due to the small size and the PBG property in the photonic crystal, to minimize the wavelength losses in the band gap range, Bragg conditions should be used to determine the minimum rows of dielectric rods around the waveguide. To achieve these conditions, Eq. (2) is given [43]:

$$n_a d_a + n_b d_b = \frac{\lambda}{2} \quad (2)$$

where, d_a, d_b, n_a, and n_b are the diameter of the rod, the distance between rods, the refractive index of the dielectric rod, and the refractive index of air, respectively [43].

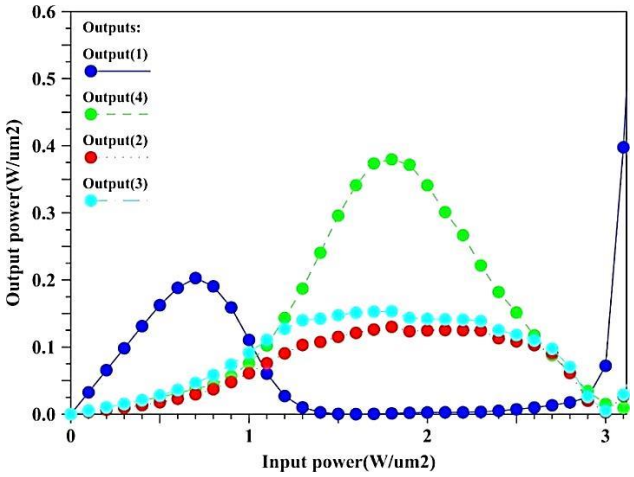

Fig. 5. Output power versus input power in the proposed power splitter (color online)

The ADC consists of two parts. There is a power splitter at the input of the ADC. These power splitters are used to control the input-to-output power using controlling rods that have radii R1, R2, and R3. The output power versus input power diagram of this splitter is depicted in Fig. 5. Due to the dependence of the controlling rods on the input power intensity, the output power of port 1 is dominant in the input power range of 0 to 1 W/μm^2. In the input power range of 1 W/μm^2 to 2.8 W/μm^2, the output power of ports 2, 3, and 4 are dominant, and finally, in the input power of 2.9 W/μm^2, the output powers of all 4 ports are the same and very low.

The second part of ADC is a 4×2 multiplexer. The controlling parameters of this multiplexer are the radius and the refractive index of coupling rods and the radius of the scattering rods. The diagram of the output powers regarding the changes in refractive index and the radius of coupling rods are shown in Figs. 6 and 7, respectively. According to Figs. 6 and 7, to achieve the proper input power from port 1, the radius and refractive index of the coupling rods should be in the range of 65 nm to 75 nm and 1.35 to 1.45, respectively. In this range, the output transmission power from port 1 creates a logic "one" state. In this case, the output power from port 2 is very low and creates a logical "zero" state.

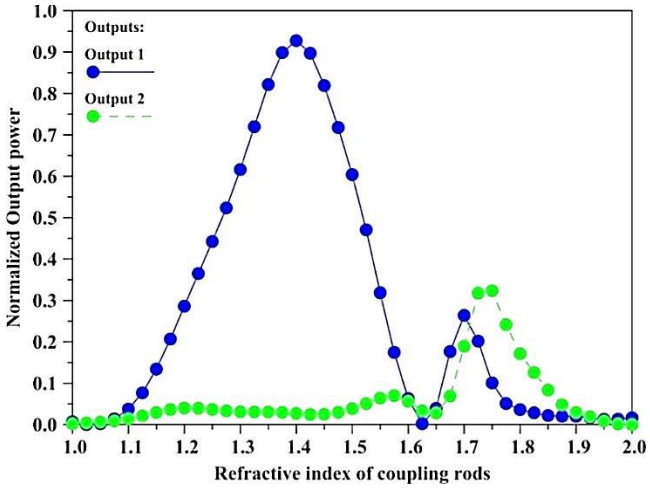

Fig. 6. Output transmission power versus refractive index of coupling rods in the proposed ADC (color online)

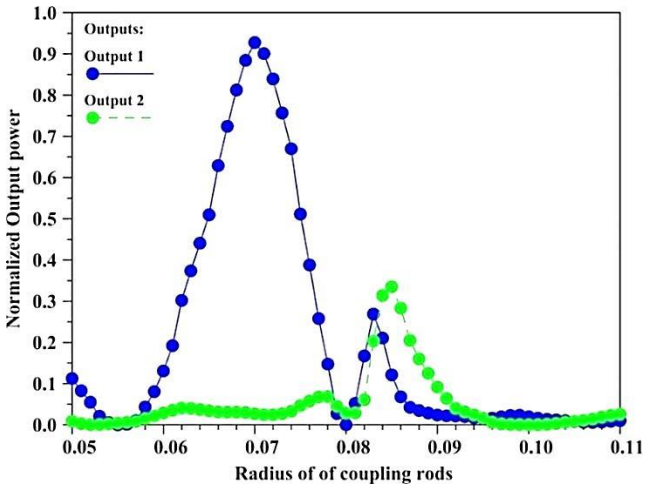

Fig. 7. Output transmission power versus radius of coupling rods (diameters are in μm) in the proposed ADC (color online)

One of the most important points in the proposed structure for analyzing the output transmission power in terms of refractive index and radius of the dielectric coupling rods is to reach a logic "one" state in port 2. As can be seen in Fig. 6, when the refractive index of the coupling rods changes in the range of 1.73 to 1.78, the transmission power of port 2 has a logic "one" state. In this case, the value of output transmission power from port 2, which causes a logic "one" state in the output of this port, is less than the output power in the optimal refractive index range mentioned above. Also, the radius of the dielectric coupling rods in the range of 83 nm to 87 nm causes a logic "one" state in output port 2, and in this case, the output transmission power is less than the optimal range of radius. In Fig. 7, the diameter of the coupling rods is in terms of micrometers.

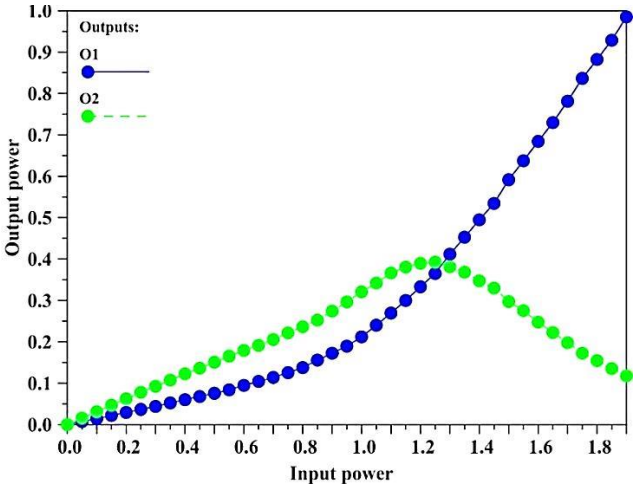

Fig. 8. Output transmission power versus input power in proposed ADC (color online)

In the proposed ADC, according to the controlling factors in the power splitter structure, and the radius and refractive index of the dielectric coupling rods in the multiplexer part of the structure, transmission power and output wavelength of the O1 and O2 ports are controlled. The trend of changes in output power from port one is almost in the form of changes in the X2 function in the positive range. The output power from port 2 has ascending changes in the input power range from zero to 1.2. As the input power increases by 1.2, the output transmission power changes decrease. A threshold level power must be defined to create the logic "zero" and logic "one" at the output of this converter which according to the mentioned power, logic codes ("zero" and "one") be determined at the O1 and O2 ports. To determine the level of threshold power the symmetry range of zero and one at the output should be considered. The symmetry of the zeros and ones in this converter increases the efficiency and application in optical integrated circuits. The threshold power for this converter is considered to be 0.17 W/μm^2. According to this level of threshold, by changing the input power from 0 to 0.497 W/μm^2, the output power of both O1 and O2 outputs is below the threshold power and logically has a value of "zero". While the input power varies in the range of 0.497 W/μm^2 to 0.848 W/μm^2, the output power of port O1 is below the threshold and the output power of port O2 is above the threshold. In this case, the logic state of ports O1 and O2 is "zero" and "one", respectively. Changes in the input power in the range of 0.848 W/μm^2 to 1.74 W/μm^2 cause a reasonable level of one in the two outputs O1 and O2. The output power of ports one and two in this case is higher than the threshold level. The maximum output power from port two occurs in this range. With changes in input power from 1.74 W/μm^2 to 2 W/μm^2, output power from port one is strongly ascending and output power from port two is descending sharply. In this case, output O1 has a logic level of "one", and output O2 has a logic level of "zero". Fig. 8 shows the output power changes from two ports O1 and O2, and Fig. 9 illustrates the field distribution profile

with respect to the input power changes from 0 to 2 W/μm^2. The logical statuses of the output ports O1 and O2 with respect to the output power of these ports are listed in Table 3.

Table 3. The "on" and "off" status of the output ports of the proposed ADC

Input power domain (W/μm^2)	O1	O2	Digital Output
0 < Pin < 0.497	0	0	00
0.497 < Pin < 0.848	0	1	01
0.848 < Pin < 1.74	1	0	10
1.74 < Pin < 2	1	1	11

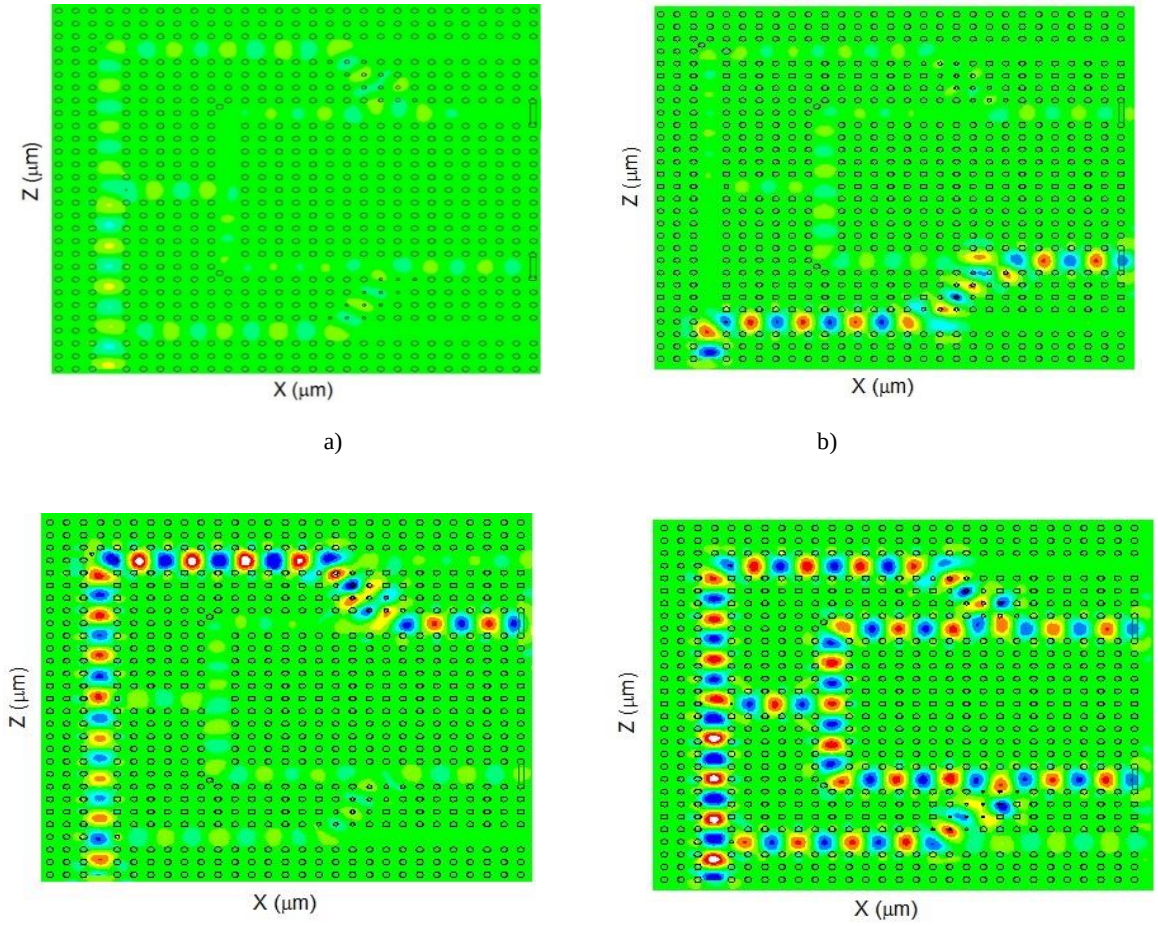

Fig. 9. The field distribution profile of the proposed ADC when the input power changes in the ranges from 0 to 2 W/μm^2. (a) O1=OFF and O2=OFF, (b) O1=OFF and O2=ON, (c) O1=ON and O2=OFF, (d) O1=ON and O2=ON (color online)

The quantified pulse width and conversion rate (speed) are among the most important parameters of the optical ADC. The quantified pulse width is calculated by [44]:

$$W_{qp} = \frac{P_{\max} + P_{\min}}{QS} \quad (3)$$

where, W_{qp} is the quantified pulse width, P_{max} is the maximum power, P_{min} is the minimum power, and QS is the number of quantization steps. To calculate this parameter, at first, the sinusoid input applies to the waveguide with different amplitudes. The rate of this converter was calculated using the time duration, in which the pulse was without distortion at the output. The time at which all outputs reach a steady state is the minimum

detectable pulse width and quantization [16]. Fig. 10, shows the response time of the two output ports of the 2-bit converter. The minimum response time was equal to 0.7 ps. Based on this time delay, the converter rate was estimated as 1430 Gb/s.

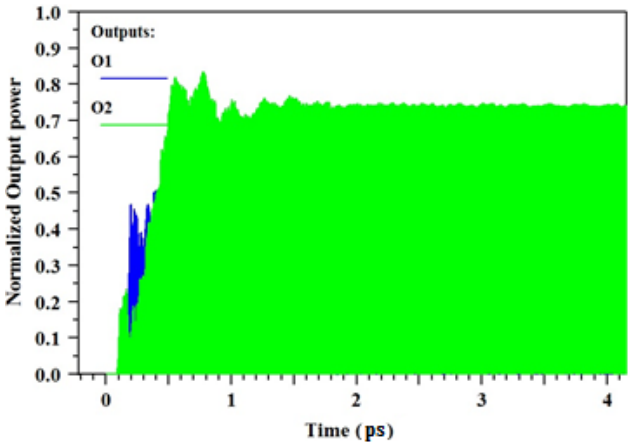

Fig. 10. Time response diagrams for the two ports of the proposed ADC (color online)

Table 4. Comparison between the proposed S-shaped ADC and other ADCs

Structure	Time delay (ps)	The output efficiency	Footprint (μm^2)
Ref [1]	5	75%	806
Ref [15]	4	84%	1785
Ref [23]	5	72%	1250
Ref [34]	1.5	85%	2016
Ref [36]	1	75%	924
Ref [45]	1	-	1796
This Work	0.7	89%	841

Table 4 compares the important parameters of the proposed structure with those of the ADCs presented in recent years. To compare the structure of all-optical analog-to-digital converters, three parameters of dimensions, speed, and noticeable difference between output power and threshold power play a key role. To prove the advantage of the suggested structure over the presented converters, the comparison of the parameters of the proposed structure with the previously presented structures are listed in Table 4. As can be seen, the delay time of our proposed converter is more suitable than the structures stated in this table. Due to the small dimensions of the proposed converter, this structure can be implemented in all-optical integrated circuits.

4. Conclusion

This study proposed a 2-bit two-dimension photonic crystal ADC, which was made of silicon dielectric rods with a linear refractive index of 3.46, square-shaped unit cells, a lattice constant of 524 nm, and a fill factor of 0.2a. To control the output power in the proposed structure, the refractive index of three dielectric rods 3.46, 3.48, and 3.50 is considered as one of the control elements. The refractive index of these dielectric rods has linear and nonlinear parts. The nonlinear part of these rods is considered 3.46 K, 3.48 p, and 3.50 s, respectively. This converter worked based on the interference principle. The threshold level of 0.17 W/μm^2 was considered to detect if the output channel power was 0 or 1. According to this threshold level, the on and off statuses of ports 1 and 2 were determined. The proposed structure was analyzed using PWE and FDTD methods. The U-shaped structure bandwidth was considered to be small to achieve the greatest change in the outputs due to the change in the input optical intensity as well as a significant difference between logic 0 and 1. The output efficiency and footprint of the proposed structure were calculated to be 80%, and 741 μm^2, respectively. Considering the minimum quantized pulse width of 0.7 ps, the converter rate of the proposed structure was obtained at 1430 Gb/s.

Acknowledgments

This work has been done in Nano-photonics and Optoelectronics Research Laboratory (NORLab), Shahid Rajaee University.

Funding

This work was supported by the Shahid Rajaee Teacher Training University under grant number 4976.

Authors' contributions

Masoud Mohammadi and Rahim Karami: designed and performed simulations and analyzed data, Mahmood Seifouri: supervised, wrote - reviewed and edited, and Saeed Olyaee: verified, edited, and prepared the final draft of the manuscript.

References

[1] F. Mehdizadeh, M. Soroosh, H. Alipour-Banaei, E. Farshidi, IEEE Photonics Journal **9**(2), 1 (2017).
[2] M. J. Maleki, Mir. A. Soroosh, Crystals **9**(12), 635 (2019).
[3] Lu Liu, Shuang Liu, Weiwen Qian, Hanzhao Li, Huilian Ma, Applied Optics **60**(23), 6755 (2021).
[4] A. Askarian, F. Parandin, Electromagnetics **43**(5), 291 (2023).
[5] A. Askarian, F. Parandin, Optical and Quantum Electronics **55**(5), 419 (2023).

[6] A. Askarian, F. Parandin, Journal of Computational Electronics **22**(1), 288 (2023).
[7] A. Askarian, G. Akbarizadeh, M. Fartash, Optical and Quantum Electronics **51**, 1 (2019).
[8] Xiaobin Xu, Ningfang Song, Zhihao Zhang, Wei Cai, Fuyu Gao, Asia Communications and Photonics Conference, Optical Society of America, paper Su1A.3 (2017).
[9] Adi Shamir, Theoretical and numerical analysis of rotating photonic crystals and the photonic crystal optical gyroscope, University of Tel-Aviv, 2006.
[10] A. Askarian, Optical and Quantum Electronics **55**(9), 822 (2023).
[11] B. Mohammadi, M. Soroosh, A. Kovsarian, Y. S. Kavian, Photonic Network Communications **38**, 115 (2019).
[12] S. M. Musavizadeh, M. Soroosh, F. Mehdizadeh, Indian Journal of Pure & Applied Physics **53**(11), 736 (2015).
[13] M. J. Maleki, M. Soroosh, A. Mir, Appl. Opt. **59**(18), 5422 (2020).
[14] A. Tavousi, M. A. Mansouri-Birjandi, Superlattices and Microstructures **114**, 23 (2018).
[15] S. Naghizade, H. Saghaei, Optical and Quantum Electronics **53**(3), 1 (2021).
[16] S. Keren-Zur, T. Ellenbogen, Nature Photonics **12**(10), 575 (2018).
[17] T. Sridarshini, S. I. Gandhi, V. N. Jannath, Ui. Firthouse, Laser Physics **30**(11), 116206 (2020).
[18] D. Jafari, T. Nurmohammadi, M. J. Asadi, K. Abbasian, Optics & Laser Technology **101**, 138 (2018).
[19] A. Askarian, G. Akbarizadeh, M. Fartash, Optik **207**, 164424 (2020).
[20] Chris H. Sarantos, Dagli Nadir, Optics Express **18**(14), 14598 (2010).
[21] Hongxia He, Chi Hao, Xianbin Yu, Tao Jin, Shilie Zheng, Xiaofeng Jin, Xianmin Zhang, Optics Communications **425**, 157 (2018).
[22] Fares S. Almehmadi, Monish R. Chatterjee, Optical Engineering **53**(12), 126102 (2014).
[23] F. Mehdizadeh, M. Soroosh, H. Alipour-Banaei, E. Farshidi, Applied Optics **56**(7), 1799 (2017).
[24] M. Mohammadi, M. Seifouri, S. Olyaee, M. Karamirad, Journal of Computational Electronics **20**, 984 (2021).
[25] R. J. Kumar, Roy J. Nath, Photonic Network Communications **34**(1), 84 (2017).
[26] H. Seif-Dargahi, Photonic Network Communications **36**(2), 272 (2018).
[27] Mojtaba Hosseinzadeh Sani, Saeed Khosroabadi, Mahshid Nasserian, Applied Optics **59**(4), 1049 (2020).
[28] S. I. Gandhi, T. Sridarshini, Laser Physics **29**(4), 046206 (2019).
[29] A. Askarian, Journal of Optical Communications, 2022, In Press 2023.
[30] A. Askarian, Journal of Optical Communications, p. 000010151520200311 (2021).
[31] I. Saber, R. Boddeda, F. Raineri, D. Sanchez, G. Beaudoin, I. Sagnes, Q. Glorieux, A. Bramati, J. A. Levenson, K. Bencheikh, J. Opt. Soc. Am. B **36**, 1823 (2019).
[32] F. Parandin, A. Sheykhian, Opt. Quant. Electron. **54**, 443 (2022).
[33] S. Iwamoto, Y. Ota, Y. Arakawa, Opt. Mater. Express **11**, 319 (2021).
[34] X. Geng, L. Zhao, Photonics and Nanostructures-Fundamentals and Applications **41**, 100817 (2020).
[35] A. Shamsi, R. Moradi, Optical and Quantum Electronics **52**(10), 1 (2020).
[36] F. Mehdizadeh, M. Soroosh, H. Alipour-Banaei, E. Farshidi, Optical and Quantum Electronics **49**(1), 38 (2017).
[37] B. Youssefi, M. K. Moravvej-Farshi, N. Granpayeh, Optics Communications **285**(13-14), 3228 (2012).
[38] A. Mohebzadeh-Bahabady, S. Olyaee, Applied Optics **59**(8), 2409 (2020).
[39] F. Mehdizadeh, M. Soroosh, Optoelectron. Adv. Mat. **9**(3), 324 (2015).
[40] R. Talebzadeh, M. Soroosh, F. Mehdizadeh, Optica Applicata **46**(4), 553 (2016).
[41] S. Bong-Shik, S. Yamada, T. Asano, S. Noda, Optics Express **19**(12), 11084 (2011).
[42] T. Daghooghi, M. Soroosh, K. Ansari-Asl, Applied Optics **57**(9), 2250 (2018).
[43] S. Nagabhushana, "Lasers and optical instrumentation", IK International Pvt Ltd, 2010.
[44] Paul W. Juodawlkis, Jonathan C. Twichell, Gary E. Betts, Jeffrey J. Hargreaves, Richard D. Younger, Jeffrey L. Wasserman, Fredrick J. O'Donnell, Kevin G. Ray, Richard C. Williamson, IEEE Transactions on Microwave Theory and Techniques **49**(10), 1840 (2001).
[45] J. Chen, F. Mehdizadeh, M. Soroosh, Hamed Alipour-Banaei, Opt. Quant. Electron. **53**, 510 (2021).

*Corresponding author: s_olyaee@sru.ac.ir